

The use of solid physical models for the study of macromolecular assembly

Michael J Bailey*, Klaus Schulten† and John E Johnson‡

The use of modern technology in the construction of accurate solid macromolecular models based on atomic coordinates and electron density functions has led us to re-examine the usefulness of physical models as tools for understanding molecular assembly and for designing detailed experimental and computational studies of the assembly process. Recent developments include the construction of new models, which have provided insights into the assembly of viruses and light harvesting complexes.

Addresses

*San Diego Supercomputer Center and Department of Applied Mechanics and Engineering Sciences, University of California at San Diego, La Jolla, CA 92037, USA

†Beckman Institute, University of Illinois, 405 North Mathew Street, Urbana, IL 61801, USA

‡Department of Molecular Biology, The Scripps Research Institute, 10550 North Torrey Pines Road, La Jolla, CA 92037, USA;

e-mail: jackj@scripps.edu

Correspondence: John E Johnson

Current Opinion in Structural Biology 1998, **8**:202–208

<http://biomednet.com/elecref/0959440X00800202>

© Current Biology Ltd ISSN 0959-440X

Abbreviations

BBV	black beetle virus
LH	light harvesting
LOM	laminated object manufacturing
RP	rapid prototyping
SFF	solid freeform fabrication
STL	stereo lithography

Introduction

This ‘opinion’ does not fit the form of most of the contributions to this volume in that it does not review and assess an area of macromolecular assembly with a significant current history. It is more of an ‘opinion’ in the traditional definition of the word — in that the authors have had experience with a new approach for constructing physical models of macromolecules and seek to demonstrate how these models have provided significant new insights into understanding the assembly of the protein molecules that form virus particles [1–5] and light harvesting complexes [6–8]. We use this review as an opportunity to provide a brief ‘ancient’ history of the development of physical models based on electron density functions and atomic coordinates, and to describe the sophisticated technology used to construct current models. We then relate our experiences with the technology mentioned above and attempt to demonstrate the fact that modern physical models are important tools that significantly extend the understanding of protein assembly available from modern three-dimensional computer-graphical analysis.

Three-dimensional models

Humans adapt well to the three-dimensional world of every day existence and three-dimensional objects and constructions are taken for granted. Most of us, however, have significant problems in visualizing three-dimensional features of virtual objects such as mathematical functions. Three-dimensional imaging of various density functions was particularly problematic until the advent of modern computer graphics. This has revolutionized our ability to visualize and understand three-dimensional images ranging from X-ray and magnetic resonance tomographs in medicine, to electron density functions derived from X-ray crystallography and cryo-electron microscopy. Prior to the development of modern graphics visualization, crystallographers were remarkably successful in representing density functions and the derived models in creative ways with physical models. Plotting electron density as contours on transparent plastic sheets that are then stacked to generate the third dimension has been, and still is, a highly effective way of visualizing the three-dimensional electron density function. This representation is still of value when requiring a global impression of electron density that is difficult to represent in a graphics system.

Constructing three-dimensional models from electron density is exceptionally problematic. A popular and effective approach of representing the surface of the molecule is the balsawood model. Construction of these models is based on contoured maps stacked on transparent Plexiglas. A contour was chosen that represents the surface and then on each section of the density a slice of balsawood that corresponded to that contour level was cut. These slices were then glued together and the composite is an accurate representation of the molecular surface. The most widely used device for constructing atomic skeleton models is the Richard’s box [9]. This device allows the model to be constructed from scale atomic model parts that are fitted into the density through the use of proper lighting and a half-silvered mirror that reflects the model into the density. This allows accurate fitting of the model parts directly to the density, with only slight distortions due to parallax. From the coordinates of such models it is possible to create other representations of the model. One of the most popular is the wire protein model, which is made using the phi psi angles derived from the coordinates of the backbone α -carbon atoms and implements a special device invented by Byron Ruben for bending the wire.

Simplified or reduced physical models of protein assemblies have long been important in illustrating the underlying features of such associations. Probably the most creative model maker in the area of virus assembly is Don Caspar. In order to visualize the concepts of quasi

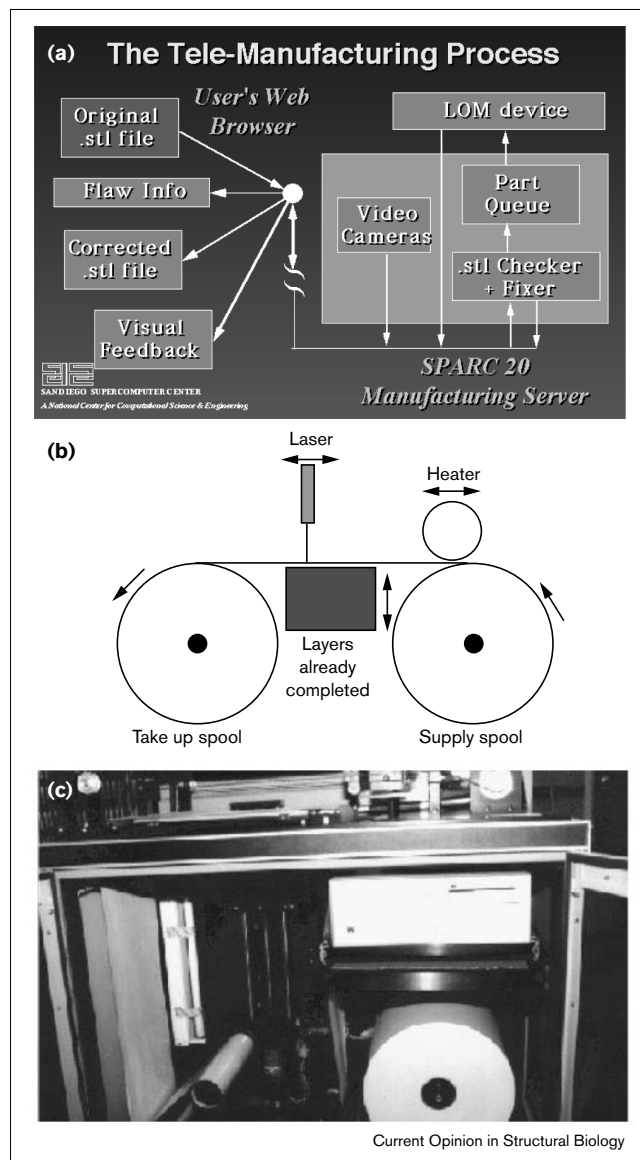
equivalence, Caspar and Klug started with paper models of icosadeltahedra [10], but then progressed to more sophisticated mechanical models that beautifully illustrate the bonding flexibility required by subunits in order to accommodate the variations in environment that occur during quasi-equivalent virus assembly [11].

Modern model fabrication

Modern computer technology has made the need for physical models less essential in the interpretation of three-dimensional structural results. It has also allowed the development of very sophisticated physical models that have provided new levels of appreciation for the complementarity of surfaces in protein assembly and have also revealed details of protein interactions that were not fully appreciated from the computer graphics representation. One of these technologies is based on a device developed for the production of prototype machine parts and has been adapted for making molecular models. The instrument produces models (in a nearly automated fashion) that are comparable to the balsawood models, but are physically robust and amenable for the study of protein associations. The input information that has been used are the coordinates of atoms of either individual subunits (light harvesting complexes and virus capsids) or a sub-assembly fragment composed of three subunits (for virus capsids). The coordinate information is converted into a list of strictly contiguous surface triangles that are used to direct the machining process. The effective resolution of the models is based on the number of triangles derived from the coordinates and, in the examples discussed below, corresponds to about 1 Å resolution. Three-dimensional models based directly on electron density would require only minor modifications compared to the procedures based on coordinates.

The principal procedure for model construction is a technology known as either rapid prototyping (RP), or solid freeform fabrication (SFF). Many technologies are used to produce these models [12–14] but regardless of the specific technology, SFF processes are all characterized by additive manufacturing methods instead of the subtractive methods as found in traditional numerical control machining. The process used at the San Diego Supercomputer Center for making solid molecular models is known as laminated object manufacturing (LOM) and is shown in Figure 1. In the LOM process, a roll of paper, available in various thickness from 0.0038 inches to 0.0100 inches, is fed a section at a time into a work area. The paper has a thin layer of glue on the underside. A hot roller (400°F) and high pressure laminate the new sheet of paper to the previous layers. A laser then cuts the outer and inner outlines of this layer as would be done in constructing a balsawood model. A series of mirrors directs the laser beam through a lens tube that is moved in x and y directions by a standard pen plotter mechanism. The power provided to the laser is carefully calibrated to slice through one and only one sheet of paper. After the laser finishes outlining

Figure 1



The tele-manufacturing process. (a) The network organization for using the tele-manufacturing facility in an interactive mode through the World Wide Web. (b) A schematic representation of the laminated object manufacturing (LOM) process. (c) A photograph of the instrument that actually manufactures the models.

the outer and inner contours of the model, it crosshatches the portions of the layer area that are not included in the two-dimensional cross section. Later on, these crosshatch cubes are removed as scrap. The process repeats for all layers until completed. The resulting model looks, feels, and acts like it is made of wood. Once a LOM model has been finished, the scrap must be removed by hand. For some models this falls right off and for some it must be dug out with dentistry-type tools.

Additive manufacturing processes have some definite advantages when fabricating three-dimensional parts for molecular

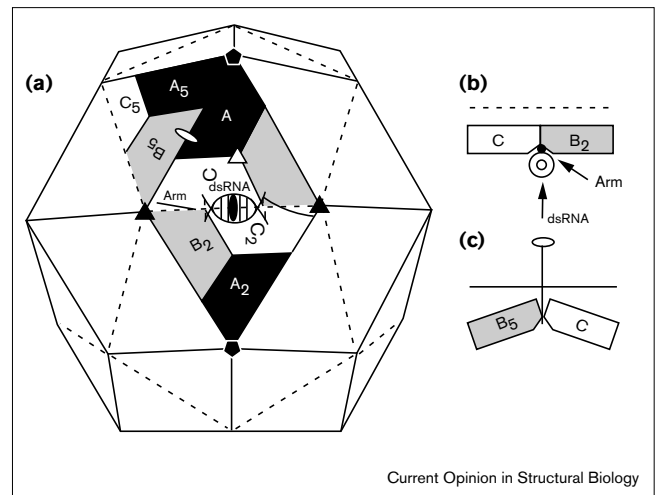
modeling. The parts can have almost arbitrary geometric complexity and the fabrication can be set up and proceed with little or no human preparation. The former is especially advantageous for making models of molecules. One of the problems with subtractive manufacturing methods is that whatever implement is doing the subtracting needs access in order to remove material. For some models, the complexity of the geometry prohibits the cutting tool getting as far in as it needs to go, or at least makes it difficult. Molecules are the ultimate example of this. Their deep channels and grooves make it almost impossible to get a machine tool into all the crevices without accidentally gouging some portion of the model that we mean to keep. The latter point is also significant. Models of molecules have both a top and a bottom that require fabrication. For typical subtractive methods, such models would need to be machined on the top and then flipped over to machine the rest. In order to flip the model over correctly, a set of fixtures and clamps would have to be designed and a process would have to be put in place to register the model once it has been flipped and clamped. This ensures that the model is indeed where the machine tool thinks it is. If this is not done, then the features on the top half will not align with the features on the bottom half. The point is that fabrication methods for molecular model making must not require much manufacturing knowledge, or they will not be used. To this end, the tele-manufacturing project is using the World Wide Web as an interface to the SFF process. As shown in Figure 1a, users can submit their geometry stereo lithography (STL) files from their favorite browser, have those files automatically checked for geometric and topological consistency, have a corrected STL file returned, or have the file queued for fabrication. When the model is being fabricated, the web page can also be used to get feedback on the manufacturing process, including seeing video images from cameras surrounding the machine.

Two examples of the use of this technology for improving our understanding of macromolecular assembly illustrate its usefulness.

Virus assembly

Nodaviruses are simple nonenveloped RNA viruses with capsids formed from a single gene product [1]. The virus particle contains 180 subunits arranged with $T = 3$ quasi-symmetry and form a polyhedron with a rhombic triacontahedron shape (Figure 2). The structures of three members of this family have been solved at near atomic resolution [5,15,16]. Black beetle virus (BBV) was chosen for study by LOM models. The icosahedral asymmetric unit corresponding to the ABC trimer shown in Figure 2 was initially constructed as a single unit (Figure 3a). Then three identical models of the A subunit were made. After some effort it was possible to assemble the three A subunits in an identical trimer corresponding to the threefold symmetric version of the ABC quasi-trimer in Figures 2 and 3a. The ABC trimer assembly demonstrated an extraordinary degree of surface complementarity not previously

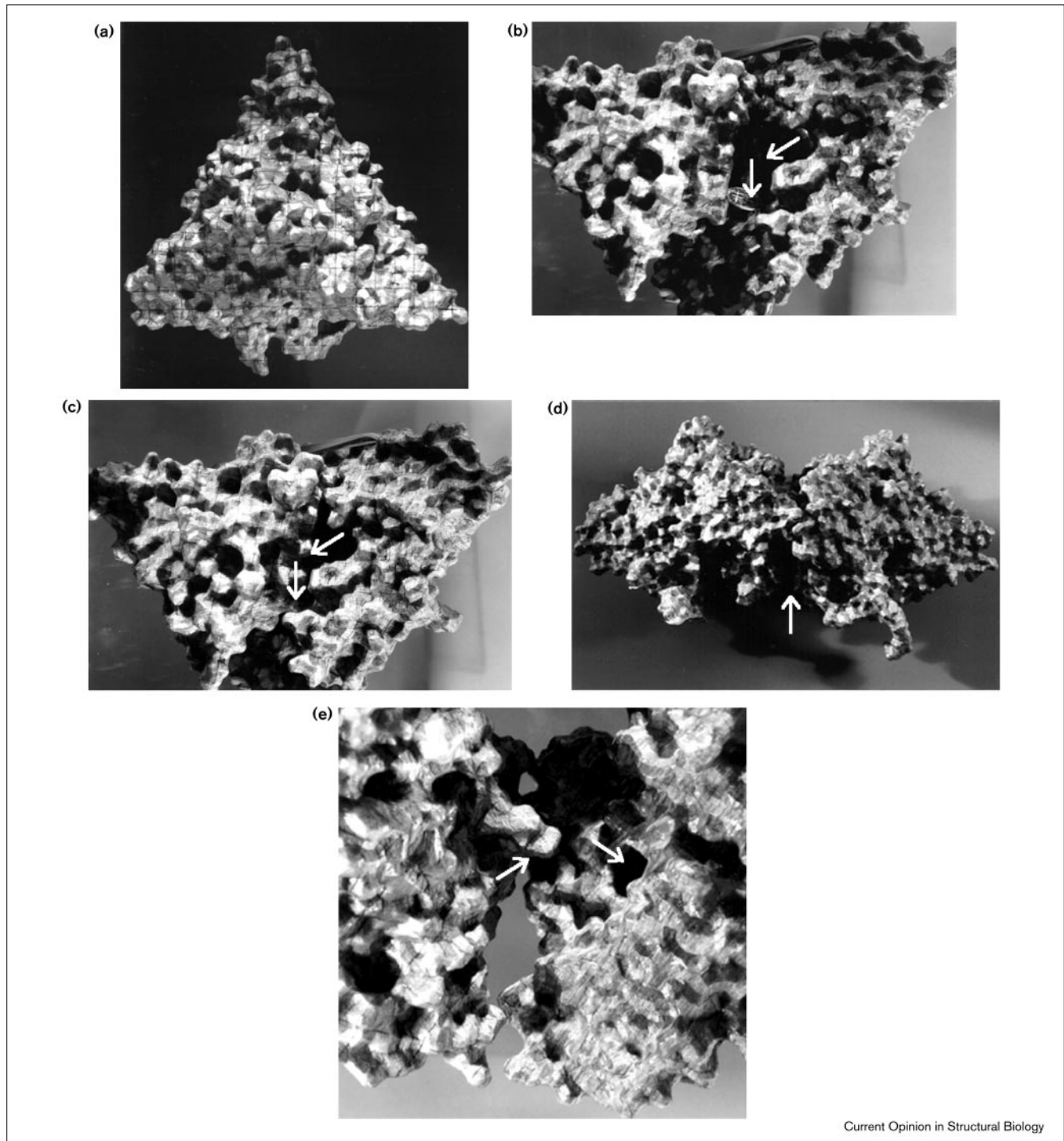
Figure 2



Schematic and physical representations of the black beetle virus. **(a)** A schematic representation of the nodavirus capsid as a rhombic triacontahedron. Each trapezoid represents a protein subunit comprising 407 amino acids. The location of duplex RNA and the polypeptide arm (residues 20–31 of the C subunit) are shown in the diagram. One icosahedral asymmetric unit is defined by the central isosceles triangle with a fivefold axis (small pentagon) at the top and threefold axes (small triangle) left and right. The labels A, B, and C represent the three subunits in each of the 60 icosahedral asymmetric units in the $T = 3$ particle. Although they are identical gene products, the subunits are not related by strict symmetry and they are structurally slightly different. Note that the A subunits cluster around the fivefold symmetry axes of the icosahedron and the B and C subunits alternate about the icosahedral threefold axes to form the quasi-sixfold axes. All subunits labeled with a letter followed by a number are related to A, B or C by an icosahedral symmetry operator indicated by the number (e.g. A_5 is related to A by an icosahedral fivefold symmetry operation). Quasi-symmetry axes relate subunits only locally to a quasi-symmetry axis (e.g. the quasi-threefold axis in the central triangle relates A, B and C with a high fidelity, but at a greater distance from the axis than it relates a fivefold axis to a quasi-sixfold axis). Each asymmetric unit has three neighboring asymmetric units. The central triangle has asymmetric units on its left and right related to it by fivefold symmetry and the third at the bottom related to it by twofold symmetry. Note that the joints (junctions between subunits) are not strictly equivalent (they are related by quasi-threefold symmetry) although the same surfaces of the protein subunits interact (e.g. the C–C₂ contact has the same protein surfaces juxtaposed as the A–B₅ contact). **(b,c)** Sideviews of the joints between asymmetric units. **(b)** The joint at the bottom of the central triangle viewed along the line connecting the two threefold symmetry axes. The dihedral angle between these two triangular surfaces is 180° (i.e. they are coplanar). **(c)** The joint at the left of the central triangle viewed along the line connecting a fivefold axis to a threefold axis. The dihedral angle between these two triangular surfaces in this polyhedron is 144° . For proper assembly to occur, the trimer interfaces must be able to hinge with a molecular switch determining the dihedral angle between asymmetric units. In the nodaviruses, the switch is a 10 base pair RNA duplex and a 12 amino acid polypeptide (residues 20–31) that are only ordered in the C subunits. These form a wedge that prevents the bending of the joint at the bottom of the central triangle.

appreciated from graphical studies or obvious from its construction as a single unit. This threefold symmetric ‘artificial’ assembly was interesting because the quasi threefold axes relate fivefold axes to sixfold axes and do not form the

Figure 3



Current Opinion in Structural Biology

Subunit interactions of black beetle virus (BBV). **(a)** A view from the exterior, down the quasi-threefold symmetry axis, of the solid LOM trimer model, constructed as a single unit with the coordinates from the A, B and C subunits of BBV. This corresponds to a single icosahedral asymmetric unit, and 60 of these units, related by icosahedral symmetry, form the BBV particle. **(b)** A view into the side of an AB interface (roughly along a line connecting the quasi-twofold axis on the bent joint to the quasi-threefold axis in the center of the triangle) formed by two identical A subunits related by threefold symmetry. The interface surface has been spread open by inserting a coin into the contact to clearly show the two juxtaposed surfaces. **(c)** The same view with the coin removed, showing the cavity formed by the two surfaces. **(d)** A view corresponding roughly to (a) showing the juxtaposition of two trimer LOM models forming a 'bent' contact. **(e)** The same view with the two trimers separated showing the 'peg into hole' alignment that guides the assembly of this interface. Given that the hole is formed by the interface of two subunits in the trimer, shown in (b) and (c), it is likely that the particles assemble from preformed trimers. Note that prior to assembly, the same interface is exposed to the twofold related 'flat' joint; however, duplex RNA and residues 20–31 of the C subunits are ordered in this interface and interrupt the 'peg into hole' interaction leading to the 'flat' contact. Indeed, residues 20–31 cover the 'peg' and part of this polypeptide inserts into the hole formed by the B_2-C_2 interface, mimicking the peptide 'peg' that inserts into the hole at the 'bent' joint.

exact threefold symmetric association seen in the particle from which the coordinates were derived. Note that two of the subunits (B and C) are associated with quasi sixfold axes whereas the third (A) is associated with the fivefold axes. This illustrates the fact that identical subunits are sufficiently similar to the quasi-equivalent subunits for an exact threefold association to be made and that there are no significant differences between threefold related AA interfaces and quasi-threefold related AB, BC, and CA interfaces. This is probably relevant to the assembly process because we hypothesize that the first fragment in assembly is an ABC trimer with exact threefold symmetry and that the observed asymmetry about the quasi-threefold axis in the assembled particle is induced during the assembly process.

After the threefold symmetric particle was made, it was noticed that a remarkable cavity was located on the surface of the trimer distal to the threefold axis (Figure 3b,c). This surface forms the fivefold and twofold associations of trimers (Figure 2). The cavities are formed by interfaces between threefold related subunits (i.e. AB, BC and CA), thus their formation depends on the assembly of the trimer. There is a perfectly complimentary protrusion on the surface of the B₅ subunit (the subunit related by a fivefold clockwise rotation to the B subunit in Figure 2) that fits into the cavity formed by the CA interface upon assembly of fivefold related trimers (Figure 3d,e), suggesting that this assembly is guided by a 'peg into hole mechanism'. Although the structure had been refined at 2.8 Å resolution and the subunit interfaces studied extensively with both computer graphics and atomic distance analysis, this remarkable complementarity had not been appreciated. Indeed, in the BBV refinement paper [3], the interaction of the cavity was included in a figure, but its full significance had escaped notice until the solid models were made.

Additional insight was gained from the assembly of the trimeric models that were constructed as a single unit (Figure 3d). It was clear that the trimeric units related by fivefold symmetry (A–B₅ contact in Figure 2) could be directly assembled as rigid bodies and form an extraordinarily complementary interface (Figure 3d,e). In contrast, when the C–C₂ association was attempted, the units could not be directly joined to form a continuous surface. This indicates that the assembly of the C–C₂ interface can not be approximated as a simple rigid-body association of assembling units, but that there are significant alterations that occur at this interface during the assembly process. The solid models led to further insights when the A–B₅ interface was compared in detail with the C–C₂ interface. Previous work showed that a 12 amino acid polypeptide (residues 20–31 of the C subunit) and 10 base pairs of an RNA duplex are ordered at the C–C₂ interface and are not ordered at the A–B₅ interface [5]. This results in a dramatic difference in the dihedral angle at the two interfaces, with the A–B₅ joint bent (144° dihedral angle) and the C–C₂ joint flat (180° dihedral angle). The solid model

shows that the ordered peptide directly interacts with the protrusion that inserts into the cavity at the A–B₅ interface and thus dramatically changes the interfacial interactions even though the same portion of the subunits are juxtaposed at the two interfaces. A portion of the ordered polypeptide actually partially interacts with the cavity at this interface, thus participating in a level of molecular mimicry that leads to quasi-equivalence.

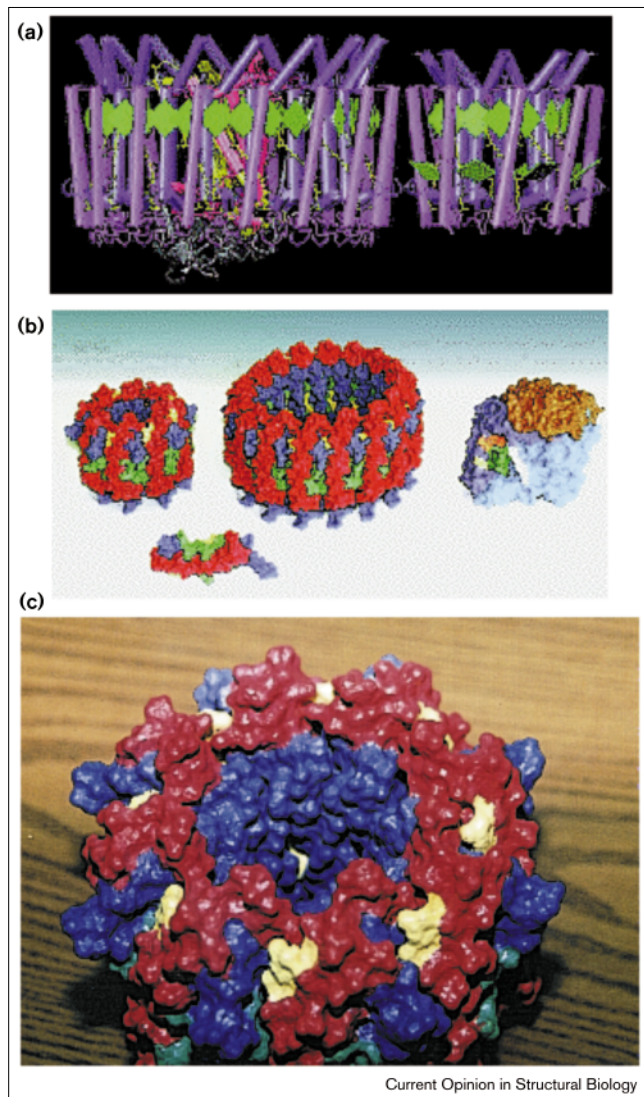
Assembly of light harvesting complexes

Light harvesting (LH) complexes, as shown in Figure 4 establish a scaffold that organizes a hierarchy of circular complexes of 300 chlorophylls and 200 carotenoids within the photosynthetic membranes of purple bacteria [8]. Organized into the form of a ring-shaped protein, LH-I, the largest light harvesting complex, surrounds a central protein complex called the reaction center. The complex of LH-I with the reaction center is in turn surrounded by about 10 smaller proteins, called LH-II, which are also ring shaped. The entire system, the photosynthetic unit, absorbs sunlight, efficiently transfers the excitation energy within a few picoseconds from the periphery to the reaction center and converts the energy into a membrane potential.

The remarkable overall architecture of the photosynthetic unit is matched by the equally remarkable architecture of the individual LH-I and LH-II complexes. LH-II of *Rhodospirillum rubrum* is composed of 16 independent peptides (eight identical α subunits and eight identical β subunits), 24 chlorophylls and eight carotenoids [7]. These components self-aggregate within the cytoplasmic membrane, most probably into heterodimers first, each made of an α apoprotein, a β apoprotein, three chlorophylls and a carotenoid, and then using the heterodimers as building blocks for assembly into a ring of eight heterodimers. In the case of LH-II from both *Rhodospseudomonas acidophila* [8] and *Rhodobacter sphaeroides* [6], nine heterodimers aggregate into the LH-II complex. The LH-I complex consists of sixteen heterodimers that each contain, however, two chlorophylls and one carotenoid.

In order to understand how the self-aggregation of the individual LH-I and LH-II complexes and the whole photosynthetic unit is achieved from its main building blocks, the $\alpha\beta$ heterodimers, we resorted to LOM models. We thought of several questions regarding the self-aggregation process to investigate with such models. How do geometry and energetics contribute to the aggregation of a single pair of heterodimers? How is this aggregation guided within the cell membrane? How do the single heterodimer building blocks control the overall ring size? How do changes of ring size affect the stability of an overall complex? These questions might be pursued through modeling calculations, but due to the large size of the overall ring systems and the qualitative nature of the phenomenon of self-aggregation, that is, one does not know *a priori* which observables to monitor, an approach through LOM models appeared more promising and certainly

Figure 4



Molecular graphics and laminated object manufacturing (LOM) representations of light harvesting (LH) complexes. **(a)** LH complexes I (LH-I, left) and II (LH-II, right), with LH-I surrounding the (barely visible) reaction center. The protein complexes are presented schematically as cylinders (α helices), tubes (coils), green squares (chlorophylls) and yellow liquorice (carotenoids). The (inner ring) α subunits are in blue, the (outer ring) β subunits are in magenta. The figure illustrates how LH-I and LH-II act as a scaffold that holds rings of chlorophylls in place as well as carotenoids. Chlorophylls and carotenoids absorb sunlight and transfer its energy to the reaction center. **(b)** LOM models of an individual heterodimer (bottom), LH-II (left), LH-I (middle) and a reaction center (right). The LH-I and LH-II models were colored as follows: α apoproteins, blue; β apoproteins, red; chlorophylls, green; carotenoids, yellow. The LH-II shown (left) is an aggregate of eight heterodimers like the one shown at the bottom; LH-I (middle) is an aggregate of sixteen heterodimers. The reaction center has been colored brown, light blue and dark blue according to its three protein subunits; ubiquinones are colored white. The LOM model of the reaction center (right) fits tightly but comfortably inside the LOM model of the LH-I ring (middle). **(c)** The fully assembled model of the LH complex.

surfaces by inspection of single surfaces, leading to an overemphasis of a few readily recognizable binding hot spots as an explanation for adhesion between proteins.

Once the LOM models of (initially) nine heterodimers had been manufactured, we decided to paint the models as shown in Figure 4. The colors helped us greatly in both the use of the models and the interpretation of our ‘hands on’ experiments. The first such experiment, the assembly of LH-II from eight heterodimer units was possibly the most revealing. It turned out that the aggregation of the building blocks did not require any flexibility of the dimer surfaces; the individual components naturally fit together tightly without the need for a flexible adjustment of their surfaces. This feature implies a favorable entropy of aggregation, that is the heterodimers do not need to explore much conformational space in order to interlock.

The resulting complex strikes the observer with the realization that the heterodimers have purposefully evolved corrugated self-complementary surfaces in order to both steer the aggregation process and to stabilize the eventual aggregates. Any coarse graining of atomic level surface features of LOM models deteriorates adhesion between heterodimers. In fact, the LOM models require about 30,000 triangles for the proper representation of the surface features of each heterodimer. This corresponds to below angstrom resolution and proved necessary in order to properly represent the relevant complementarity of surfaces.

The heterodimers are composed of two, rather short, trans-membrane helices, a feature that requires the heterodimers to be oriented strictly normal to the membrane plane; a tilt would immerse the polar side groups into the hydrophobic phase of the lipid bilayer. A pronounced top to bottom asymmetry of the heterodimer favors a vectorial orientation in the membrane. Manipulation of two heterodimer models that are properly juxtaposed and rotated relative to each other readily reveals the proper interlocking geometry of a heterodimer pair. A similar one-dimensional (rotation around the membrane normal) search process is likely to govern the rapid self-assembly of LH-II within the cytoplasmic membrane.

One can readily build rings of slightly ‘wrong’ sizes, for example, an LH-II ring of only seven units or of nine units, that is, one too few or one too many. In both cases the LOM models reveal a loose packing with wobbling heterodimer units. This is certainly a feature that results from the fact that the heterodimer LOM models stem from an eight ring structure, that is, a structure optimized for that particular ring size. The model demonstrates clearly, however, that the complementarity and orientation of the corrugated surfaces of the individual heterodimers are precise enough to control the overall ring size at eight units.

faster than simulations. It is also notoriously difficult to recognize complementary features between binding

The models revealed some altogether unexpected features. It was known that LH-II *in vivo* actually binds sixteen

carotenoids, rather than only eight as seen in the crystal structure. During the crystallization procedure half of the carotenoids, that is, one carotenoid per heterodimer, stray away. Inspection of the model revealed a channel between heterodimer surfaces into which one can fit the missing carotenoid. This feature, that is, a deviation from perfect complementarity, was not detected by means of molecular graphics, even though we had searched extensively for possible binding sites for the additional carotenoids.

We have also built the LH-I complex from sixteen LOM models of the respective heterodimers, and a LOM model of the reaction center. This allowed us to build a key section of the photosynthetic unit [6]. The LOM models revealed that one can readily clap the LH-I ring over the reaction center leading to the unique geometry of the complex. In this complex, LH-I forms an atrium-type space adjacent to the reaction center surface with the entrance of a functionally important quinone-binding site. One also notices that the sixteen unit LH-I ring is considerably more flexible in its shape than is the eight unit LH-II ring; it does not appear likely that the LH-I ring would assume its proper size and shape without the reaction center template.

Conclusions

The use of modern technology in the construction of highly accurate solid macromolecular models based on atomic coordinates and electron density functions has led us to re-examine the usefulness of physical models as tools for understanding molecular assembly and for designing detailed experimental and computational studies of the assembly process. The solid models have sensitized us to the complimentary surface features of protein subunits and their interactions. By physically assembling the models we have refined our perspectives on assembly. We now see that assembly of the nodavirus particle is guided by 'peg into hole' interface alignments that can occur only after the trimer subassembly product has formed and that the size and stability of LH complexes are as a result of highly structured corrugated associations between subunits. These observations strongly suggest that assembly pathways are dictated by associations determined by large-scale surface complementarity and that these are only supplemented by the favorable local interactions that had previously dominated our attention in both of these structures. With these observations in mind, we are pursuing qualitatively more informed computational studies of LH in order to determine the nature of the adhesion forces governing self-assembly. Experimental studies of nodaviruses are currently underway that are designed to identify drugs that interfere with assembly, or actually disassemble virus particles by binding with high affinity into the 'alignment holes' at the subunit interfaces. Similar efforts will attempt to confound the molecular mimicry that is essential for quasi-equivalent assembly. Finally, we are computationally examining the associations within other known virus structures to see if the assembly principles identified for nodaviruses are

more widely applicable and if they will lead to viable targets for the design of antiviral agents.

Acknowledgements

The tele-manufacturing of laminated object models is supported by a National Science Foundation grant, MIP-9420099 (to MJB). Studies of nodaviruses are supported by a National Institutes of Health grant GM34220 (to JEJ) and the studies of the light harvesting protein complexes are supported by the National Institutes of Health (NIH grant P41RR05969), the National Science Foundation (NSF grant BIR 9318159 and NSF grant BIR9423827) as well as by the Carver Charitable Trust (to KS). Dru Clark (San Diego Supercomputer Center) is gratefully acknowledged for his role in the tele-manufacturing of the physical models and we thank Vijay Reddy for his help in preparing Figures 2 and 3.

References and recommended reading

Papers of particular interest, published within the annual period of review, have been highlighted as:

- of special interest
 - of outstanding interest
1. Johnson J, Reddy V: **Structural studies of noda and tetraviruses.** In *The Insect Viruses*. Edited by Miller L, Ball L. New York: Plenum; 1998: in press.
 2. Reddy V, Giesing H, Morton R, Kumar A, Post C, Brooks C, Johnson J: **Energetics of quasi-equivalence: computational analysis of protein-protein interactions in icosahedral viruses.** *Biophys J* 1998, **74**:546-558.
 3. Wery J, Reddy V, Hosur M, Johnson J: **The refined structure of an insect virus at 2.8 Å resolution.** *J Mol Biol* 1994, **235**:565-586.
 4. Cheng R, Reddy V, Olson N, Fisher A, Baker T, Johnson J: **Functional implications of quasi-equivalence in a T=3 icosahedral animal virus established by cryo-electron microscopy and X-ray crystallography.** *Structure* 1994, **2**:271-282.
 5. Fisher A, Johnson J: **Ordered duplex RNA controls capsid architecture in an icosahedral animal virus.** *Nature* 1993, **361**:176-179.
 6. Hu X, Damjanovic A, Ritz T, Schulten K: **Architecture and function of the light harvesting apparatus of purple bacteria.** *Proc Natl Acad Sci USA* 1998, in press.
 7. Koepke J, Hu X, Muenke C, Schulten K, Michel H: **The crystal structure of the light harvesting complex II (B800-850) from *Rhodospirillum rubrum*.** *Structure* 1996, **4**:581-597.
 8. McDermott G, Prince S, Freer A, Hawthornthwaite-Lawless A, Papiz M, Cogdell R, Isaacs N: **Crystal structure of an integral membrane light-harvesting complex from photosynthetic bacteria.** *Nature* 1994, **367**:614-621.
 9. Richards F: **The matching of physical models to three dimensional electron density maps: a simple optical device.** *J Mol Biol* 1968, **37**:225-230.
 10. Caspar D, Klug A: **Physical principals in the construction of regular viruses.** *Cold Spring Harb Symp Quant Biol* 1962, **27**:1-24.
 11. Caspar D: **Movement and self control in protein assemblies: quasi-equivalence revisited.** *Biophys J* 1980, **32**:103-135.
 12. Bailey M: **The use of solid rapid prototyping in computer graphics and scientific visualization.** In *SIGGRAPH Course Notes for The Use of Touch as an I/O Device for Graphics and Visualization*. Edited by Spencer S. New York: ACM Press; 1996.
 13. Burns M: *Automated Fabrication*. Engelwood Cliffs, New Jersey: Prentice-Hall; 1993.
 14. Johnson J: *Unified Description of All Free Form Fabrication Technologies Based on Fundamental Principles*. Irvine, California: Palatino Press; 1994.
 15. Hosur M, Schmidt T, Tucker R, Johnson J, Gallagher T, Selling B, Rueckert R: **Structure of an insect virus at 3.0 Å resolution.** *Proteins* 1987, **2**:167-176.
 16. Zlotnick A, Natarajan P, Munshi S, Johnson J: **Resolution of space group ambiguity and the structure determination of nodamura virus to 3.3 Å resolution from pseudo R32 (monoclinic) crystals.** *Acta Crystallogr* 1997, **53**:738-746.